Enhanced performance of microbial electrolysis cells using microstructured electrodes

Erhöhte Leistungsfähigkeit mikrobieller Elektrolysezellen durch Einsatz mikrostrukturierter Elektroden

T.M. Keil[1], D. Windisch[1], V. Joukov[1], J. Niedermeier[2], W. Schulz[1], J. Albrecht[1]

A microbial electrolysis cell is set up with the purpose to realize an efficient power-to-gas process. Both hydrogen production by electrolysis and biomethanization proceed in the same reactor cell. In particular, the formation of hydrogen bubbles is strongly governed by the surface properties of the used stainless steel electrodes. Here, we introduce surface topography modifications on the micron-scale to enhance the electrical transport in the cell and support charge conversion into hydrogen. Furthermore, it is analyzed if hydrogen bubble detachment can be supported to form smaller bubbles that can be efficiently converted into methane. A positive influence on the electrical transport is found and explained by a surface-controlled suppression of bio-film passivation.

Keywords: Microbial electrolysis cell **/** power-to-gas **/** surface engineering **/** microstructuring **/** bubble formation

Um einen effizienten “Power-to-Gas” Prozess abzubilden, wird eine neuartige mikrobielle Elektrolysezelle aufgebaut, in der die Teilschritte des Prozesses, sowohl die elektrolytische Wasserstoffproduktion als auch die Biomethanisierung, im selben Reaktor stattfinden. Da insbesondere die Bildung von Wasserstoffbläschen stark von der Oberflächenbeschaffenheit der Elektroden abhängig ist, werden hier mikrostrukturierte Elektrodenoberflächen eingesetzt, um Ladungsumsatz und Wasserstoffbildung zu steigern. Zudem wird untersucht, ob die Blasenablösung an der Oberfläche zu kleineren Blasen führen kann, die effizienter in Methan gewandelt werden können. Die beobachtete Verbesserung der elektrischen Transporteigenschaften kann mit einer reduzierten Biofilmpassivierung erklärt werden.

Schlüsselwörter: Mikrobielle Elektrolysezelle **/** Power-to-Gas **/** maßgeschneiderte Oberflächen **/** Mikrostrukturierung **/** Blasenbildung

[1] Forschungsinstitut für Innovative Oberflächen FINO, Aalen University, Beethovenstraße 1, 73430 AALEN, GERMANY
[2] Institut für Materialforschung Aalen IMFAA, Aalen University, Beethovenstraße 1, 73430 AALEN, GERMANY

Corresponding author: J. Albrecht, Forschungsinstitut für Innovative Oberflächen FINO, Aalen University, Beethovenstraße 1, 73430 AALEN, GERMANY,
E-Mail: joachim.albrecht@hs-aalen.de

1 Introduction

The power-to-gas technology converts excess electric currents generated by volatile sources into storable methane gas. This is considered as a promising contribution to suppress effects of global warming through greenhouse gases such as carbon dioxide since the methane production consumes environmental carbon dioxide [1]. This might counteract the unprecedented enormous combustion of fossil fuels and emission of greenhouse gases. Currently, some large-scale Power-to-Gas systems operate in a process with two spatially separated conversion steps: first, water electrolysis and, second, biological methanization [2–4]. Challenges in creating a competitive concept are an increase of the overall efficiency, consequent upscaling and limiting the specific costs [5].

In this context significant advantages might arise from a concept that combines the individual steps in a single reactor vessel. An electrolysis cell is combined with a biologically active filling to realize the formation of hydrogen and subsequently methane with a relatively low power demand. These cells are typically called bio-electrochemical cell or microbial electrolysis cell [6–10].

There is a wide diversity in reactor architectures due to the application and function of the required system. It can be distinguished in a single-vessel versus a two-compartment reactor. Furthermore, various systems operate by means of a proton-exchange-membrane as a separation placed between anode and cathode. However, laboratory microbial electrolysis cells conveniently produced methane without using a membrane [11, 12]. To keep complexity small we follow the suggested approach within this work.

Applicability for bio-electrochemical systems is widespread and ranges from gaseous fuel extraction in sewage treatment plants to treatment of pollutants or heavy metals accumulating in industrial wastewater. Desalination of seawater or obtaining different kinds of substantial resources are upcoming topics. Microbial electrolysis cells display a multi-faceted platform technology but actually most systems have not yet passed the scientific laboratory stage [13–16]. Challenges in upscaling are related to the efficiency of the bio-electrochemical cells. For a profound gas production it is inevitable to realize a constant high conversion of electric charge to gas. Low ohmic losses are required for adequate productivity and contribute to a more competitive energy transformation concept [17, 18].

The formation of passivating layers through physisorption of organic substances on the surface of the electrode, especially the cathode strongly increases the ohmic losses. This biofilm formation contributes immensely to the electric charge transport resistance after an operation of several months. Similar but less prominent biofilm formation has been found on anodes as well [19–22].

In addition to physisorptive processes passivation is caused by chemical reactions at the surface of the electrode during operation. Salt precipitation predominantly occurring at the cathode leads to an enormous drop in power density on the long-term operation. Energy dispersive x-ray spectroscopy identify sodium carbonates and calcium carbonates as predominantly deposited materials [23–26].

Finally, it has to be taken into account that the formation of gas bubbles at the surface leads to a reduction of the active surface. The area that is occupied by a gas bubble does not support charge conversion. To increase effectivity it is highly desired to release gas bubbles as quick as possible from the surface of the electrode [27–30]. In microbial electrolysis cells an additional advantage is apparent. A reduction of the size of released bubbles leads both to an increase of the surface-to-volume ratio and to an enhanced dwell time when rising through the biologically active filling. The subsequent methanization benefits significantly from both processes.

2 Experimental

In this work we use a single-chamber vessel at laboratory dimensions with a volume of 1.7 litres, *Figure 1*. Within this set-up we introduce stainless steel electrodes with different surface topography. Two process steps should in particular be affected by this surface modification. First, the size distribution of formed hydrogen bubbles is modified, second, the process of passivation either by physisorption or chemisorption can change.

We use electrodes inside the microbial electrolysis cell made of stainless-steel 1.4301 (X5CrNi18-10). The active area is kept constant to

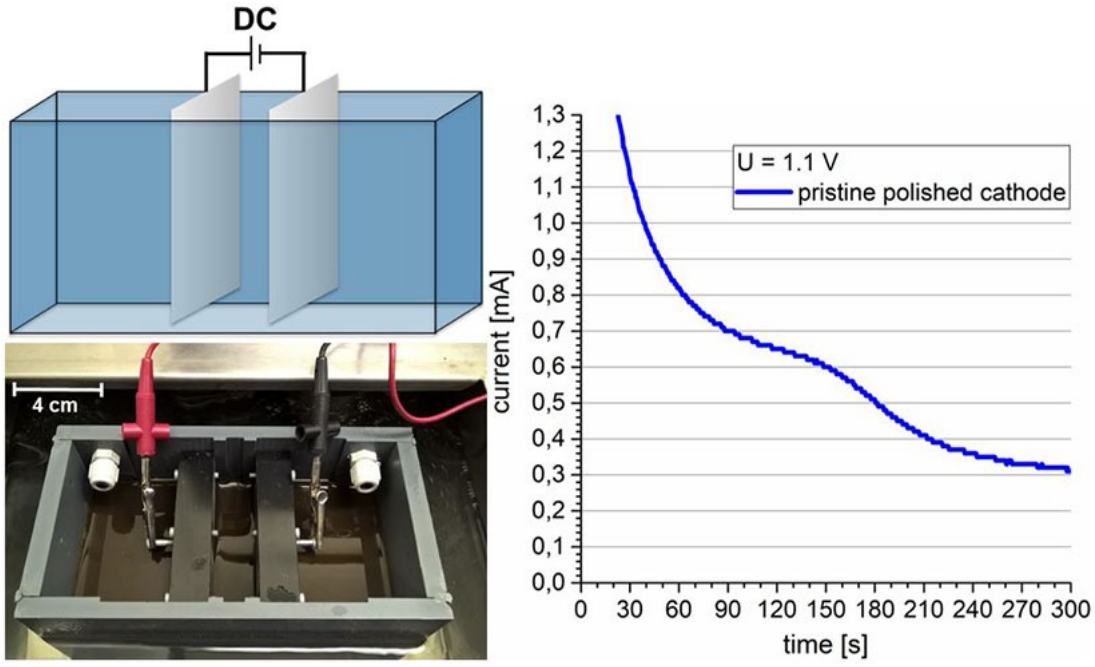

Figure 1. Sketch (top left) and photograph (bottom left) of the used microbial electrolysis cell in laboratory dimensions for direct current. The graph on the right displays the measured electric current over time for a polished electrode under constant voltage level $V = 1.1$ V.

be 90×90 mm^2. Within this study three different surface topographies are investigated that are generated by different mechanical treatment. The electrodes are inserted into the laboratory reactor vessel to conduct a bio-electrochemical process. Therefore, a fixed anode and various cathodes were positioned in a distance of about 40 mm in a vessel filled with water diluted biomass as an electrolyte at a temperature of 39 °C–42 °C, Figure 1, left. The representative biomass sample batch has been extracted from an agricultural fermentation plant for biogas production. It consists mainly of excrement of farm animals with some remains of grass and corn plants. The biomass is sieved to remove solid particles with sizes larger than 2 mm and water-diluted by a factor of 2 to 3.

The first experiment is carried out with a polished electrode. In this configuration a direct current voltage of $V = 1.1$ V is applied and the evolving electric current is measured over a period of typically 5 minutes. The right panel displays the recorded electric current.

It is found that the electrical current strongly decays with time. Initially observed transport currents of more than 1 mA drop to a value of about 0.3 mA after 300 seconds of operation. The electric current over time curve shows an additional feature. There is a two-step behaviour found characterized by a first strong decrease of the observed current in the beginning of the experiment up to about $t = 60$ s. A second drastic decrease sets in at about $t = 150$ s. This suggests two different processes that are responsible for the observed decay of the electric current.

Operating stainless steel electrodes in microbial electrolysis cells can typically lead to the formation of different types of passivating layers that are formed at the surface. One the one hand, it is found that chemical surface reactions lead to the formation of carbonate layers on electrodes in microbial electrolysis cells [23–26]. In addition, mass transport initiated by the electric field in the electrolyte in many cases leads to the formation of weakly bound biofilms consisting of microorganisms and water [19–22]. The fact that a two-stage drop of the electrical current is observed supports the idea that the two steps refer to these two kinds of films that might develop during operation.

3 Results

To distinguish between different kinds of film deposition we perform selective cleaning or reactivation processes after operation of the cell. Measuring the electric current during 5 minutes of operation leads to significantly varying results for particular pretreatment procedures, *Figure 2*. The sequence in the left panel contains measurements at $V = 1.1$ V of a pristine polished electrode (mid blue), of a used electrode after 4 runs of 5 minutes each (light blue) and after a mechanical cleaning step using isopropanol and a brush (dark blue). In the right panel the final cleaning step is substituted. Here, chemical etching in 2 M nitric acid for 10 minutes is carried out (purple).

The first (mid blue) and second (light blue) curve look very similar for both of the used electrodes. The electric current for the pristine electrode shows a two-stage drop, the initial current is reduced from values larger than 1 mA to values of 0.2 mA to 0.3 mA after 5 minutes. The second current drop sets in after an equivalent period of about $t = 150$ s. After 4 cycles of operation with a duration of 5 minutes each we find a strong suppression of the overall current to values that are significantly smaller than the final current at $t = 5$ minutes in the pristine curve. In addition, there is no sign of a multi-stage process. The suppression of the current has obviously continued during the additional cycles. We have to clarify that all curves show large initial values that rapidly decay within a few seconds. These are related to the charging of the metal electrodes (capacitive current) and do not contribute to the charge conversion.

Significant differences occur when considering the consequences of the final cleaning step, respectively. In case of the mechanical procedure (dark blue, left panel) we find a small recuperation of the current values, for all times the current is smaller than for the initial pristine surface. When introducing the chemical etching step (purple, right panel). The recovery is much larger, the purple curve even ends at current values at $t = 300$ s that are larger than the initial mid blue curve.

These results strongly suggest that the current suppression has to be described by the already mentioned two-stage process. First, chemical surface reactions lead to the formation of carbonate films that are responsible for the first drop of the electric current. Second, on top of the carbonate film a jelly-like biofilm develops. This process sets in after some delay (about 150 s) and is responsible for the second observed current drop.

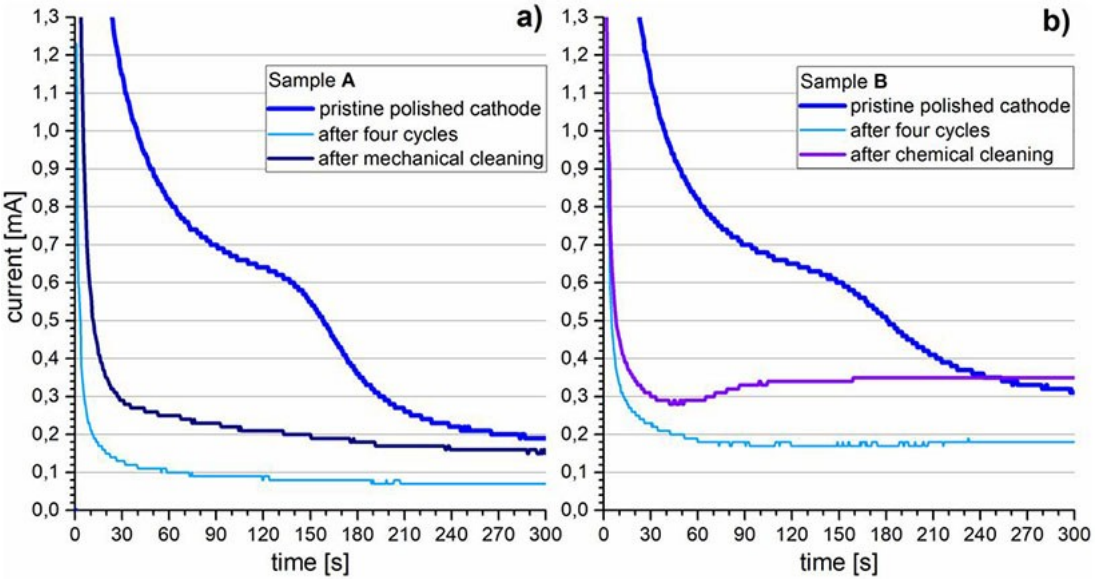

Figure 2. Development of the electric transport current at $V = 1.1$ V after different pretreatments. The left panel depicts the current development within 5 minutes of the pristine electrode (top curve, mid blue), after 4 cycles of operation (5 minutes each, bottom curve, light blue) and finally after mechanical cleaning (middle curve, dark blue). In contrast, the right panel depicts results obtained at a similar electrode. Here, the mechanical cleaning step is replaced by a chemical etching step (middle curve, purple).

When applying different recovery processes, namely, a mechanical and a chemical one, the films will react in a different manner. The mechanical cleaning under isopropanol will only affect the physically bound biofilm and remove it completely. Analogue results are obtained by different mechanical treatments such as scrapping it with spatulae or moving magnets [31, 32].

Since the carbonate layer is hardly affected by such procedures the current recuperation is expected to be rather small. Performing the chemical etching step, the chemically bound carbonate layer will be removed as well and the current recuperation will be larger. This is what we observe in the experiment. Similar observations are made when using various diluted hydrochloric or acetic acids as etching solution [33, 34].

The results lead to the conclusion that the suppression of the charge transport is originated by the passivation of the surface of the electrodes, Figure 2. Two processes are responsible for the reduced charge conversion which is accordingly found in similar works. First, a thin carbonate film develops at the surface that significantly reduces the electrical conductivity and second, the contact to the water-based biomass in the reactor leads to the formation of a biofilm also suppressing the electrical conductivity [19–26]. The biofilm covers the surface by a physisorption process and can therefore be removed by classical mechanical cleaning.

Now, the role of a modified surface topography of the electrodes is studied. For that purpose we use three different kinds of electrodes that are generated by different mechanical treatment. First, a mechanically polished surface, second, a surface containing unidirectional microgrooves created by mechanical grinding and, finally, a microembossed surface. The latter surface has been prepared using a stamp with prominent microdiamonds partially embedded in a nickel matrix on top of a tungsten carbide base material that is pressed onto the steel surface. The diameter of the diamonds is 25 µm leading to an according size of individual imprints [35, 36].

The surface of the three types of electrodes has been examined using white-light interferometry, *Figure 3*.

The false color representation maps depict the height distribution of the surface on an area of about $800 \times 800\ \mu m^2$. The displayed topographies clearly show the striking differences of the used surfaces. Electrode (A) exhibits a surface roughness of about $R_q = 0.08\ \mu m$. This hardly visible in the image with a height scale from -3 µm to 3 µm. In case of electrode (B) we find pronounced, scar-like grooves with typical widths of the order of 10 microns and above and a statistically distributed individual depth ranging from 1 micron to 5 microns. There is a rough parallel orientation of the structures. Surface (C) shows statistically distributed imprints with lateral sizes of about 20 microns an individual depth up to 5 microns. It is interesting to note that the modified surface fraction in case of electrode (C) is of the order of only 5 %.

The performance of the different electrodes is evaluated in an equivalent experiment in the microbial electrolysis cell for 5 minutes. In the left panel

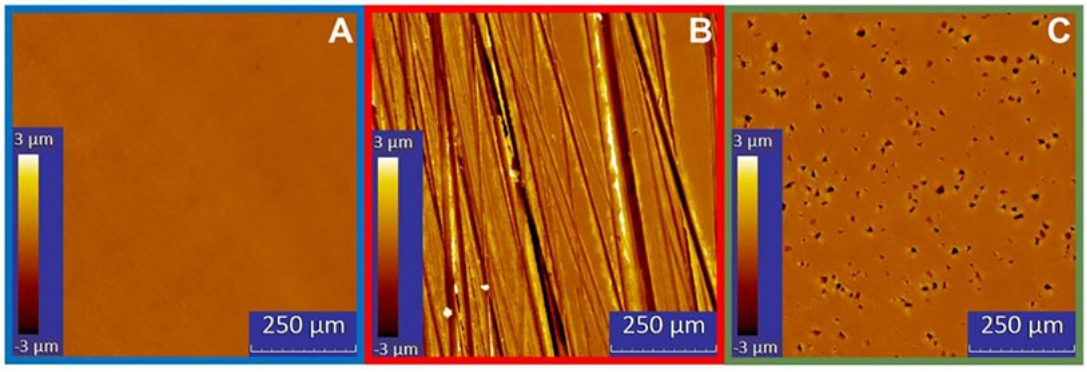

Figure 3. Interferometry images of the surface topography of three different stainless steel electrodes. The left panel (A, blue) displays the surface of the polished electrode acing as reference. (B, red) depicts a surface containing unidirectional grooves from mechanical grinding and (C, green) a microembossed surface.

a polished electrode and an electrode containing mechanical grooves are compared, *Figure 4*. The right panel illustrates the behavior of a (different) polished and a microembossed electrode. All surfaces are directly prepared before the experiment.

We find a clear increase of the electric current for electrode (B) compared to electrode (A) over the whole measurement period (left panel). Interestingly, the difference between both curves is variably pronounced at different stages of the process. Between $t = 60$ s and $t = 160$ s an increase of about 20 % is found. The effect of the modified surface is rather small. After about $t = 160$ s – when the second current drop in case of the polished reference electrode sets in – the modified electrode (B) nearly preserves the electric current of $I = 0.6$ mA. Finally, after $t = 300$ s a current enhancement by a factor of two is found. In this regime, the modified surface of electrode (B) effectively suppresses a current drop. Comparing electrodes (A) and (C) in the right panel of Figure 4 we find a different behaviour. The blue and the green curve exhibit a similar shape, the observed currents are even slightly higher in the case of the polished electrode. The small difference is most pronounced before $t = 160$ s. With longer operation time the difference is probably not significant. It is comparable to differences that occur between the left and the right blue curve that should nominally show an identical shape.

The introduction of surface structures strongly affects the detachment of produced gas bubbles. The population of gas bubbles at the surface significantly reduces the active area of the electrode. If bubble formation plays a role for the observed increase of the electric transport, size and number should differ for the electrodes, Figure 3. We observe the formation of bubbles by optical microscopy. Here, we use an enhanced DC voltage of $V = 3.5$ V to directly compare the performance of the electrodes in case of pure water and water-diluted biomass. The set-up consists of a horizontally oriented electrode and a ring-shaped counter electrode on top. The surface of the electrode is observed when applying the voltage and the size distribution of detaching bubbles is measured, *Figure 5*.

In case of water (left panel) there is the expected significant difference in size distribution for all three tested electrodes. The polished surface (blue curve) generates bubbles with typical diameters between 100 µm and 400 µm with a maximum at around 250 µm. The surface with microgrooves (red) produces bubbles with diameters between

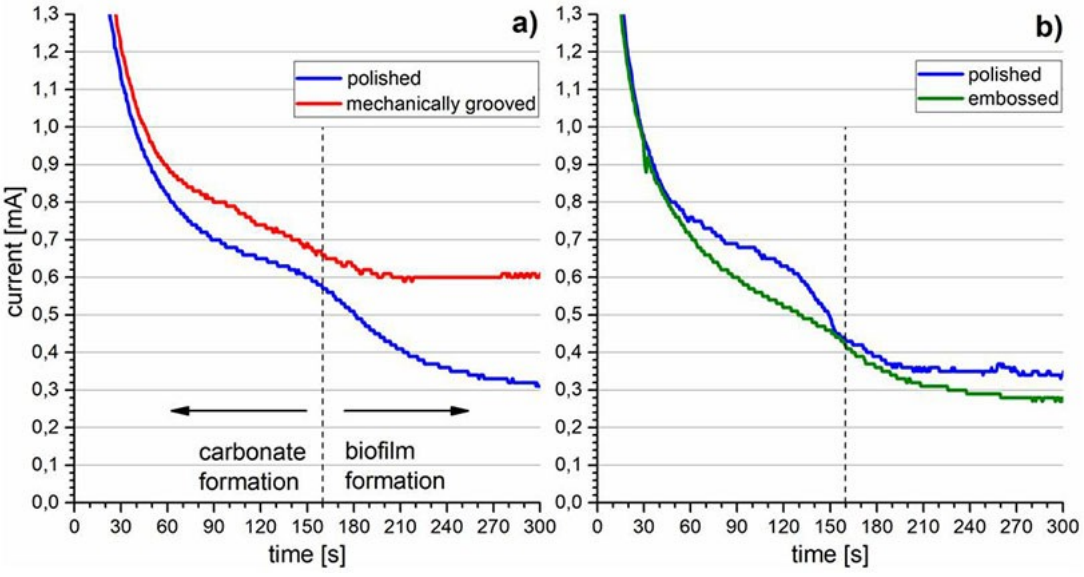

Figure 4. Left: Initial current curves of a polished (A, bottom curve, blue) and mechanically grooved electrode (B, top curve, red) directly after preparation. Right: Corresponding curves of a polished (A, top curve, blue) and an embossed electrode (C, bottom curve, green). The experiment is performed under constant voltage $U = 1.1$ V in the microbial electrolysis cell. The dashed vertical line at $t = 160$ s separates two regimes where dominantly the carbonate film and the biofilm is deposited, respectively.

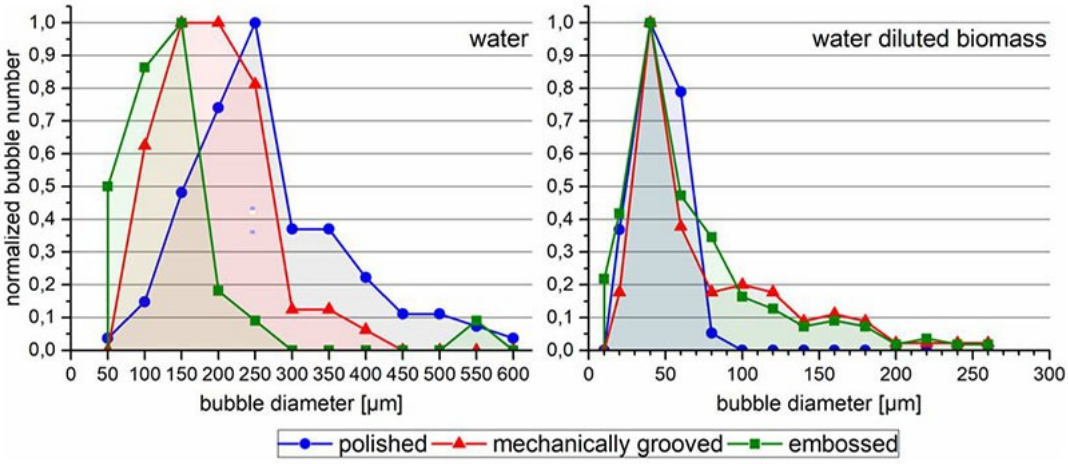

Figure 5. Distribution of bubble sizes in water (left panel) and water diluted biomass (right panel) at a direct current voltage of $V = 3.5$ V. Note, that the x-axis of the right panel is enlarged by factor of two.

75 µm and 300 µm with a pronounced maximum at 175 µm and, finally, the microembossed surface exhibits a size distribution with a maximum at 150 µm. As expected, we find a clear influence of the surface topography on the size distribution of the generated gas bubbles. In particular, the microembossed surface shows the largest effect which is attributed to sharp edges of the imprints that act as nucleation sites.

This behaviour changes when filling the cell with water-diluted biomass. Here, we find in all cases narrow size distributions with particular maxima of about 40 µm and maximal sizes below 200 µm. An appropriate explanation can found when considering the precipitation driven formation of a gas bubble. In case of the "clean" water filling the inhomogeneities at the surface of the electrode are mainly responsible for the formation of bubbles. In case of the "dirty" biomass filling the majority of nuclei for bubble formation are provided by solid particles in the inhomogeneous biomass suspension. Additional nuclei on the surface hardly influence this process any further. With these results we can clearly rule out the bubble formation process as origin of the current enhancement in case of the micro-grooved electrode. As a consequence, the passivation of the surface electrode by the formation of chemically and physically bound films seems to be the only reason for the increase in charge conversion in case of the microstructured surfaces.

An important information is provided by the pronounced increase of the electric current during the second drop of the current curves that is observed in case of the microgrooved surface. Referring to the model that two different passivation films develop on the surface the introduction of the grooves seems to affect in particular the formation of the second film, namely the physically bound biofilm.

A very simple model is able to reasonably describe the observed results. The introduced modification of the surface topography affects the adhesion of particles, in particular, when the typical dimensions of particle and surface structures are similar. Micrographs were taken of the surface of the cathodes in the pristine state, after the formation of the carbonate film and finally after the formation of a biofilm, *Figure 6*.

Considering the surface before and after the formation of the carbonate layer we find that the surface topography is conserved. This is typical for a chemical deposition process that is evaluated on the length scale of microns.

The microscope panel on the right shows the surface after the microorganisms have attached and the biofilm is formed. A blurry surface has developed after 5 minutes that does not exhibit the original surface features anymore. Since the typical size of the particles in the biofilm is of the order of several microns the original surface topography is covered.

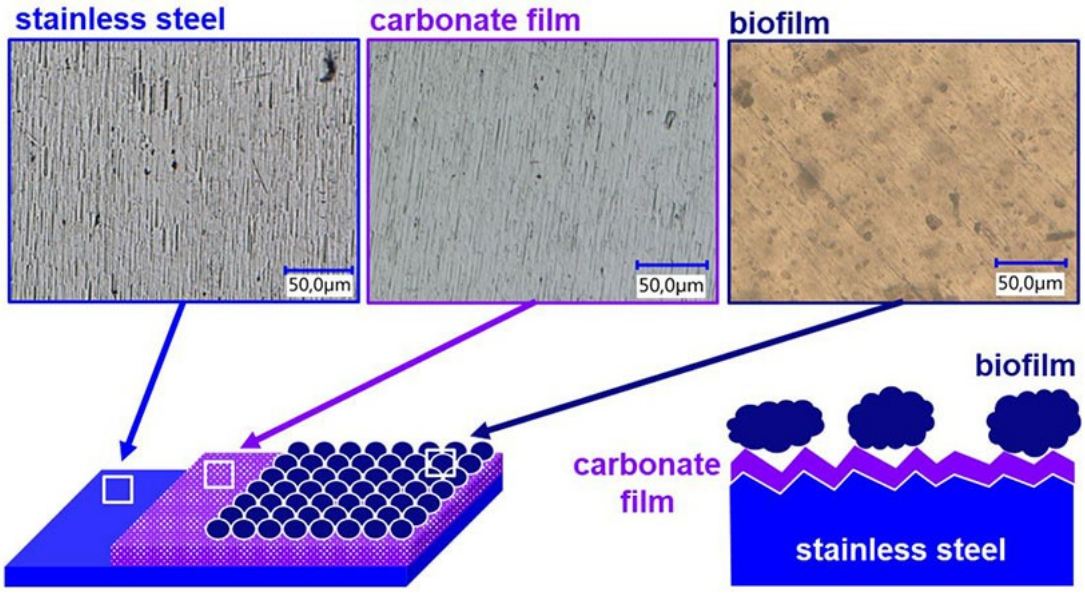

Figure 6. The top row depicts micrographs of the surface of the cathode after preparation (left), after the deposition of the carbonate film (centre) and after the biofilm has formed (right). The bottom row shows a sketch of the film surface (left). The right panel illustrates how surface roughness leads to a reduced adhesion in case of the microorganisms forming the biofilm.

In this simple picture it is reasonable that the modified surfaces of the electrodes shown in Figure 3 affect the formation of the passivating films in a different manner. The carbonate film grows by the deposition of individual molecules. Locally, the attachment process is not influenced by surface modifications on the length scale of microns. Carbonate deposition can be described in a similar way as snow covers mountains. In both cases the topography is conserved. A different scenario is found in case of the attachment of bioparticles. Since the size of the particle is larger than the modifications of the surface topography an incomplete contact area is formed. The surface structures avoid the formation of a continuous interface between particle and electrode. This is comparable to the well-known Lotus effect of (super-) hydrophobic surfaces [37]. The cross-sectional sketch on the right in Figure 6 illustrates this in a simplified way. The carbonate layer completely covers the surface irrespective of a surface modification on the micron scale. The attachment of large particles forming the biofilm is affected by the surface structures. The incomplete interface that evolves leads to a significant reduction of the adhesion forces. This explains the reduced performance of the microembossed surface as well. Since the modified surface area of these electrodes is only of the order of 5 % there is enough space flat enough to warrant the attachment of bioparticles and film deposition is hardly affected. This additionally supports the result that bubble formation that benefits from microembossing plays only a minor role. This dominant process is passivation by growing biofilms. The fact that their formation on stainless steel electrodes can be suppressed by a mechanical surface treatment is a welcome alternative to the usage of chemically active inhibitors that might not be permitted in particular applications.

4 Conclusions

We investigated the influence of mechanically structured stainless steel electrodes on the performance of a microbial electrolysis cell. The set-up realizes a complete power-to-gas process in one vessel filled with natural, water-diluted biomass. It is found that the electrical transport is strongly suppressed with operation time in two steps that are attributed to a two-step passivation process. Subsequently, a carbonate film and a biofilm are deposited on the cathode.

The insertion of mechanically structured cathodes reduces the electric current suppression and improves the performance of the cell. This finding

is not related to a modified hydrogen bubble formation at the surface of the cathode that is found when operating the cell with water. The inhomogeneity of the bio-mass suspension offers enough nuclei for bubble formation and detachment, additional structures at the surface do not contribute significantly.

The enhancement of the electrical currents can be explained by suppression of passivation. In particular, it is found that appropriate surface structures hinder the deposition of a water-based biofilm. We attribute the main effect to the presence of a high density of sharp groves that are generated by the mechanical treatment of the surfaces.

Since biofilm formation is typically controlled by adding inhibitors to the electrolyte the results of this work might offer a chemical-free alternative in some cases.

Acknowledgement

We thank M. Berbic, S. Lindenlaub, P. Pfundstein and M. Hofmann from Aalen University for valuable discussions.

5 References

[1] M. Specht, M. Sterner, B. Stürmer, V. Frick, B. Hahn, *DE Patent 102009018126 A1* **2009**.

[2] M. Jentsch, T. Trost, M. Sterner, *Energy Procedia* **2014**, *46*, 254.

[3] M. Sterner, Bioenergy and renewable power methane in integrated 100 % renewable energy systems: Limiting global warming by transforming energy systems, Kassel University Press, Kassel, **2009**.

[4] M. Specht, J. Brellochs, V. Frick, B. Stürmer, U. Zuberbühler, M. Sterner, G. Wallstein, *Erdöl Erdgas Kohle (EEK)* **2010**, *126*, 342.

[5] G. Leonzio, *Waste Biomass Valorization* **2019**, *1*.

[6] H. Liu, S. Grot, B.E. Logan, *Environ. Sci. Technol.* **2005**, *39*, 4317.

[7] R.A. Rozendal, H.V.M. Hamelers, G. Euverink, S. Metz, C. Buisman, *Int. J. Hydrog. Energy* **2006**, *31*, 1632.

[8] R.A. Rozendal, C.J.N. Buisman, *WO Patent 2005005981* **2005**.

[9] B.E. Logan, K. Rabaey, *Science* **2012**, *337*, 686.

[10] D.R. Bond, D.E. Holmes, L.M. Tender, D.R. Lovley, *Science* **2002**, *295*, 483.

[11] B.E. Logan, D. Call, S. Cheng, H.V.M. Hamelers, T.H.J.A. Sleutels, A.W. Jeremiasse, R.A. Rozendal, *Environ. Sci. Technol.* **2008**, *42*, 8630.

[12] P. Clauwaert, W. Verstraete, *Appl. Microbiol. Biotechnol.* **2009**, *82*, 829.

[13] Y. Zhang, I. Angelidaki, *Water Res.* **2014**, *56*, 11.

[14] J.M. Foley, R.A. Rozendal, C.K. Hertle, P.A. Lant, K. Rabaey, *Environ. Sci. Technol.* **2010**, *44*, 3629.

[15] Q.I. Roode-Gutzmer, D. Kaiser, M. Bertau, *ChemBioEng Rev.* **2019**, *6*, 209.

[16] H. Alhimali, T. Jafary, A. Al-Mamun, M.S. Baawain, G.R. Vakili-Nezhaad, *Biofuel Res. J.* **2019**, *6*, 1090.

[17] A. Ceballos-Escalera, D. Molognoni, P. Bosch Jimenez, M. Shahparasti, S. Bouchakour, Á. Luna Alloza, A. Guisasola, E. Borràs, M. Della Pirriera, *Applied Energy* **2020**, *260*, 114138.

[18] R. Rousseau, L. Etcheverry, E. Roubaud, R. Basséguy, M.-L. Délia, A. Bergel, *Applied Energy* **2020**, *257*, 113938.

[19] L. Koók, P. Bakonyi, F. Harnisch, J. Kretzschmar, K. Jung Chae, G. Zhen, G. Kumar, T. Rózsenberszki, G. Tóth, N. Nemestóthy, K. Bélafi-Bakó, *Bioresour. Technol.* **2019**, *279*, 327.

[20] M. Oliot, L. Etcheverry, A. Bergel, *Bioresour. Technol.* **2016**, *221*, 691.

[21] M.L.K. Sulonen, A.-M. Lakaniemi, M.E. Kokko, J.A. Puhakka, *Bioresour. Technol.* **2016**, *216*, 876.

[22] J.-H. Tian, R. Lacroix, E. Desmond-Le Quéméner, C. Bureau, C. Midoux, T. Bouchez, *bioRxiv* **2019**, 609909.

[23] J. An, J. An, N. Li, L. Wan, L. Zhou, Q. Du, T. Li, X. Wang, *Water Res.* **2017**, *123*, 369.

[24] M. Santini, S. Marzorati, S. Fest-Santini, S. Trasatti, P. Cristiani, *J. Power Sources* **2017**, *356*, 400.

[25] M. Santini, M. Guilizzoni, M. Lorenzi, P. Atanassov, E. Marsili, S. Fest-Santini, P. Cristiani, C. Santoro, *Biointerphases* **2015**, *10*, 031009.
[26] M. Sugnaux, M. Happe, C.P. Cachelin, A. Gasperini, M. Blatter, F. Fischer, *Chem. Eng. J.* **2017**, *324*, 228.
[27] P. Chandran, S. Bakshi, D. Chatterjee, *Chem. Eng. Sci.* **2015**, *138*, 99.
[28] R. Hreiz, L. Abdelouahed, D. Fünfschilling, F. Lapicque, *Chem. Eng. Res. Des.* **2015**, *100*, 268.
[29] T. Rauscher, C.I. Müller, A. Gabler, T. Gimpel, M. Köhring, B. Kieback, W. Schade, L. Röntzsch, *Electrochim. Acta* **2017**, *247*, 1130.
[30] H. van Parys, S. Van Damme, P. Maciel, T. Nierhaus, F. Tomasoni, A. Hubin, H. Deconinck, J. Deconinck, *WIT Trans. Eng. Sci.* **2009**, *65*, 109.
[31] R. Rossi, W. Yang, E. Zikmund, D. Pant, B.E. Logan, *Bioresour. Technol.* **2018**, *265*, 200.
[32] E. Zhang, F. Wang, Q. Yu, K. Scott, X. Wang, G. Diao, *J. Power Sources* **2017**, *360*, 21.
[33] R. Rossi, X. Wang, W. Yang, B.E. Logan, *Bioresour. Technol* **2019**, *290*, 121759.
[34] R. Rossi, W. Yang, L. Setti, B.E. Logan, *Bioresour. Technol.* **2017**, *233*, 399.
[35] M. Kommer, T. Sube, A. Richter, M. Fenker, W. Schulz, B. Hader, J. Albrecht, *Surf. Coat. Tech.* **2018**, *333*, 1.
[36] T. Sube, M. Kommer, M. Fenker, B. Hader, J. Albrecht, *Tribol. Int.* **2017**, *106*, 41.
[37] A.B.D. Cassie, S. Baxter, *T. Faraday Soc.* **1944**, *40*, 546.

Received in final form: January 8th 2021

ARTICLES

A power-to-gas process is set up inside a single microbial electrolysis cell where both hydrogen production and biomethanization are realized. Microstructured stainless steel electrodes inside the vessel can significantly improve the electric transport. This is attributed to an inhibition of biofilm formation on the surface. A desired reduction of bubble sizes for better conversion is not observed.

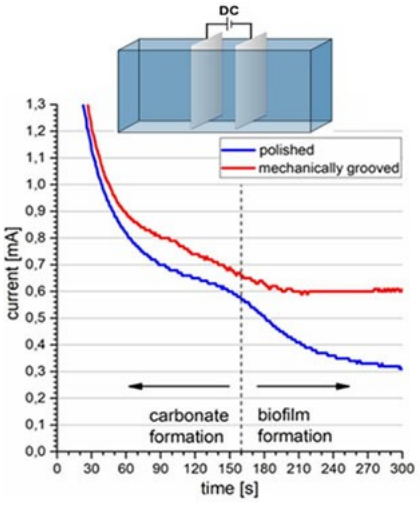

T.M. Keil, D. Windisch, V. Joukov, J. Niedermeier, W. Schulz, J. Albrecht*